Midlatitude ionospheric plasma temperature climatology and empirical model based on Saint Santin incoherent scatter radar data from 1966 to 1987

Shun-Rong Zhang, John M. Holt, and Angela M. Zalucha[1]

Haystack Observatory, Massachusetts Institute of Technology, Westford, Massachusetts, USA

Christine Amory-Mazaudier

Centre for the Study of Earth and Planets Environments (CETP), CNRS, Saint-Maur-des-Fossés Cedex, France

[1]   Ionospheric plasma temperature variations have recently been studied based on incoherent scatter radar (ISR) observations at a lower midlatitude site, Shigaraki, in East Asia [*Otsuka et al.*, 1998] and Millstone Hill, a typical subauroral midlatitude site in North America [*Zhang and Holt*, 2004]. The French Saint Santin ISR, with a geographic latitude slightly higher but an apex latitude $14°$ lower than Millstone, collected bistatic and quadristatic measurements for over two solar cycles beginning in September 1965. A database of these data, containing observations between 1966 and 1987, has been used in this study in order to establish the midlatitude ionospheric climatology, in particular that of the upper atmosphere thermal status, as well as empirical models for space weather applications. This paper presents, in comparison with the Millstone Hill results, variations of ion and electron temperatures (T_i and T_e) with solar activity, season, time of the day, and altitude. The F2 region T_e at St. Santin is found to be lower than at Millstone between March and July, when the St. Santin electron density N_e is relatively higher. The midday T_e below 300 km increases with F10.7, as at Millstone Hill. Above 300 km it tends to decrease with F10.7 at St. Santin, while it increases in summer at Millstone Hill. T_i between 250 and 350 km peaks midway between spring and summer. We have also created St. Santin ionospheric models for N_e, T_e, and T_i using a bin-fit technique similar to that used for the Millstone Hill models. Comparisons with corresponding IRI predications indicate good agreement in T_i at high solar activity, and above the F2 peak, T_e from the IRI tends to be higher than both the St. Santin and Millstone Hill models.   *INDEX TERMS:* 2443 Ionosphere: Midlatitude ionosphere; 2447 Ionosphere: Modeling and forecasting; 2467 Ionosphere: Plasma temperature and density; 0358 Atmospheric Composition and Structure: Thermosphere—energy deposition; 6952 Radio Science: Radar atmospheric physics; *KEYWORDS:* ionospheric plasma temperatures, ionospheric climatology, empirical model, incoherent scatter radar, St. Santin

1.   Introduction

[2]   On the basis of data from in situ experiments and incoherent scatter radar (ISR) experiments, a general physical understanding of the upper atmospheric thermal status has been reached as reviewed by, e.g., *Schunk and Nagy* [1978]. Owing to a limited amount of data, outstanding issues exist in more specific but important topics such as the solar and geomagnetic activity dependency, the altitude dependency, and a quantitative specification for modeling purposes. The latest efforts addressing these and other issues have been reported by *Otsuka et al.* [1998], who used the middle and upper (MU) atmosphere radar incoherent scatter observations of ion and electron temperatures (T_e and T_i) at Shigaraki in East Asia during 1986–1997, and by *Zhang and Holt* [2004, hereinafter referred to as Paper I], who used ISR data at Millstone Hill from 1970 onward for their climatology and modeling studies. In this latter work, diurnal and seasonal variations and solar activity dependency were presented and compared to the

---

[1]Now at Department of Earth, Atmospheric, and Planetary Sciences, Massachusetts Institute of Technology, Cambridge, Massachusetts, USA.

International Reference Ionosphere (IRI) model [*Bilitza*, 2001] and the Te and electron density Ne interrelationship was discussed. That seems to be the longest dataset (~3 solar cycles) so far analyzed. At an L value of 3, Millstone Hill lies in the vicinity of the magnetic field lines passing through the plasmapause boundary and has often been considered "subauroral." In this North American region the fact that the geomagnetic latitude is about 12° higher than the corresponding geographic latitude may cause high conductivities, and thermospheric circulations over this near-magnetic pole site may lead to interesting ionospheric variations [*Rishbeth*, 1998] which differ from what is seen at other longitudes.

[3] The French Saint Santin (44.6°N, 2.2°E) ISR, with a geographic latitude slightly higher but an apex latitude 14° lower than Millstone and an L of 1.8, collected bistatic and quadristatic measurements for over two solar cycles beginning in September 1965 [*Bauer et al.*, 1974]. Previous studies on the the ionospheric plasma temperatures above the St. Santin radar have focused on the daytime energy balance to understand the altitude variation [e.g., *Lejeune and Petit*, 1969], the nocturnal high Ti over Te phenomena [*Mazaudier and Bauer*, 1976], and the Ne and Te relationship [*Lejeune and Waldteufel*, 1970; *Lejeune*, 1972]. Many efforts have been made to study the thermospheric composition and temperature including the exospheric temperature, all of which are based on the Ti and Te observations [see *Alcaydé et al.*, 1978, and references therein]. These thermospheric results have been compared with those from Millstone Hill by, e.g., *Salah et al.* [1976], who showed a general similarity in the exosphere temperature for the two sites. *McPherson and Oliver* [1997] compared St. Santin plasma temperatures with the Malvern ones and found overall similarity but considerable difference in detail in terms of diurnal and seasonal changes.

[4] This paper presents the F2 region Te and Ti climatology and empirical model based on all available St. Santin data taken during 1966–1987. We will discuss various variations including local time, seasonal and altitude variations and the solar activity dependence, and the Te and Ne coupling, in comparison with Millstone Hill results obtained previously for 1970–2001. A description of St. Santin radar empirical models including Te and Ti will be given and comparisons with the latest IRI model will also be presented.

2. Data Statistics

[5] The St. Santin data are archived in the CEDAR database. They were imported into the *Madrigal* database system hosted by the MIT Millstone Hill Observatory and entered into our analysis after filtering out obviously bad data, e.g., temperatures <150°K or >5000°K or the temperature ratio Tr = Te/Ti > 5, etc. We have used all available data without specifying measurement modes. Typically, the F2 region profile data are provided at a 25 km interval, the E region data are provided at a 5 km interval, the E−F region data are provided at a 10–15 km interval, and the well-above F2 peak region data are provided at a 50 km interval. Most of the data come with an error estimate; for those without an error estimate we assign a large value which is
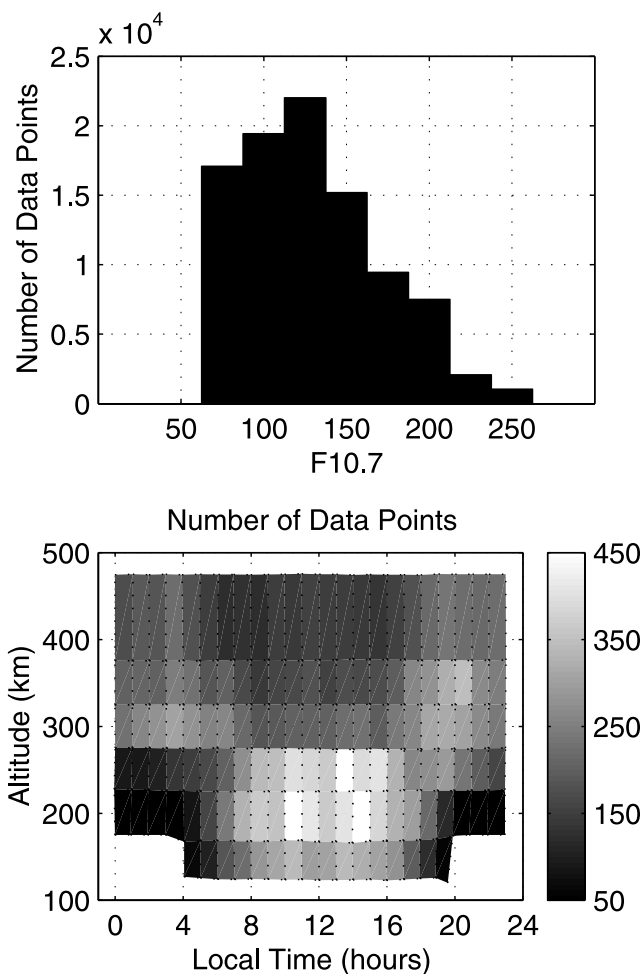

Figure 1. Data point distributions as a function of (top) F10.7 and (bottom) local time and altitude.

close to the maximum error in the corresponding data. Our statistics and modeling procedure takes into account these errors in the data.

[6] In this study the previous day's F10.7 index is used as the solar activity proxy. It was indicated by *Buonsanto and Pohlman* [1998] that the thermospheric response time to the solar activity is near to 1 day and the correlation of the thermospheric temperature with the previous day's F10.7 is slightly higher than that with F10.7 for another day, such as the current day, and even with the F10.7 81-day average. *Roemer* [1967] found the response time in neutral density to be ~1 day. Our tests with Millstone Hill Ne, Te, and Ti data spanning ~3 solar cycles show that with more data involved in the analysis, the correlations of each parameter with different F10.7 values (for the current day, 1 day or more days earlier, and the 81-day averages) are really not significantly different. While these tests indicate small difference in using different F10.7 values for statistical study purposes, we opt to the previous day's F10.7 in accord with the work of *Buonsanto and Pohlman* [1998] and *Roemer* [1967].

[7] Figure 1 shows the data point distribution for ap < 10 as a function of F10.7 and local time and altitude, indicating that the majority of data is from F10.7 < 150 units, from the

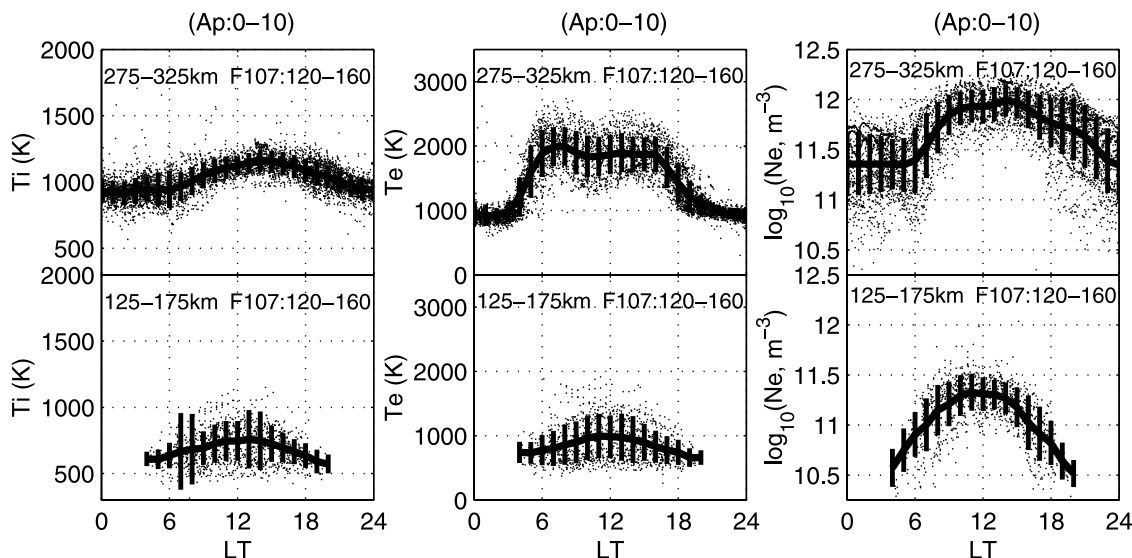**Figure 2.** Diurnal variations of Ti, Te, and Ne at two altitude ranges for F10.7 between 120 and 160 units.

F2 peak altitude which is higher at night and lower by day. Few data were available below 175 km at night.

3. Climatology

[8] Diurnal, seasonal (monthly), yearly, and altitude variations are shown in Figures 2–6 for Te and Ti (and Ne as well except in Figures 4 and 6). The diurnal variation plot (Figure 2) incorporates data from lower F region altitudes and from around the F2 peak for all months with F10.7 between 120 and 160 units. Hourly averages are given by those solid lines, and error bars show standard deviations on the averages. Ti in the F2 region approaches maximum in the afternoon, mirroring the daily bulge of the thermospheric temperature. The strong thermal coupling between neutrals, ions, and electrons makes Ti = Te below 150 km. Above 200 km, Te presents double peaks following sunrise and in the afternoon, with a lower temperature around noon when Ne is high and the electron cooling is strong. The peaks change with season, altitude, and solar activity.

[9] Figure 3 shows seasonal variations of the three parameters at lower F region altitudes and around the F2 peak for local noon, with dots representing data, solid lines representing the monthly average, and error bars represent-
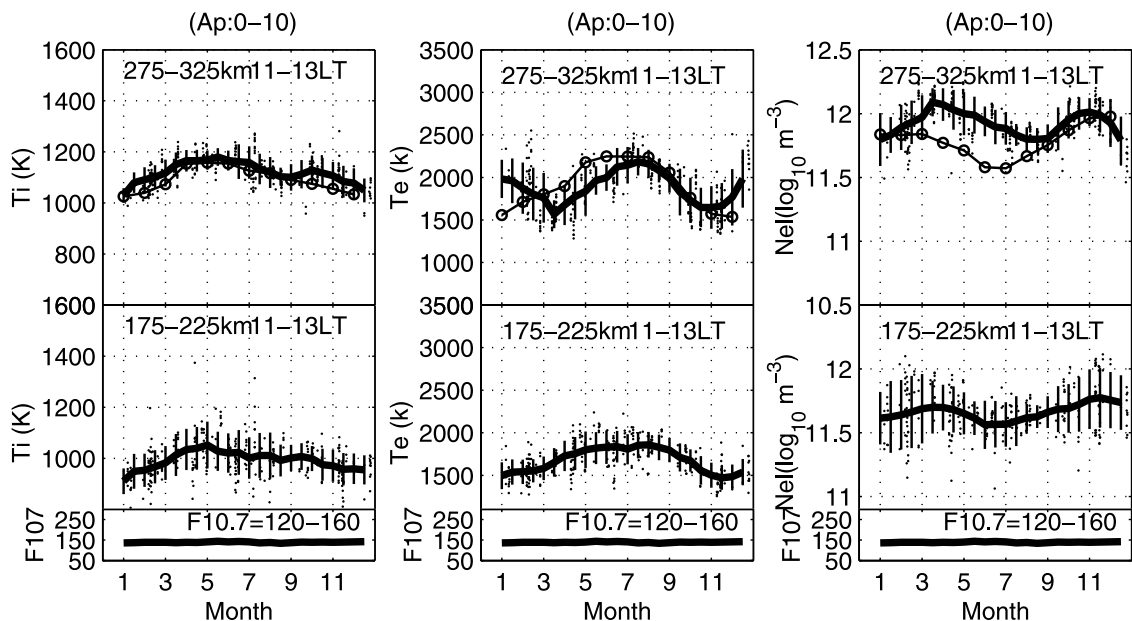

Figure 3. Seasonal variations of the midday Ti, Te, and Ne at two altitude ranges for F10.7 between 120 and 160 units. Millstone Hill empirical model values are represented by the line and circle curve for 300 km at 1200 LT with F10.7 = 140 units.
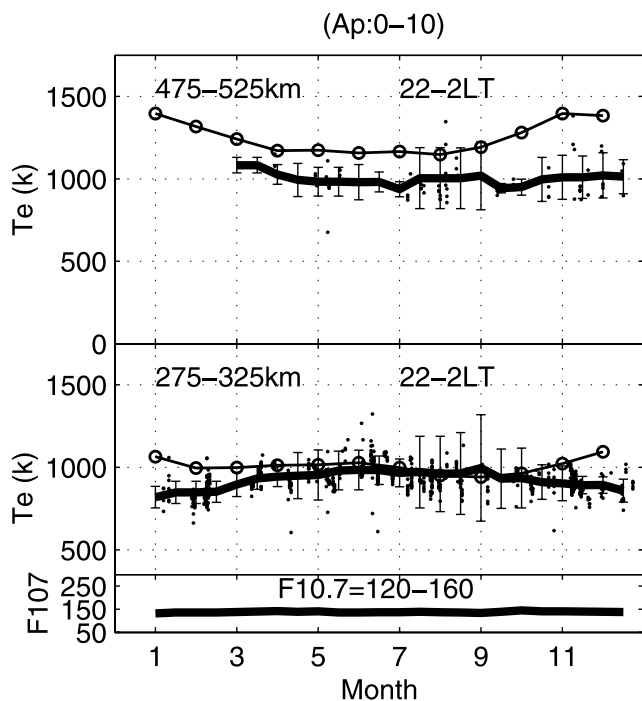
Figure 4. Seasonal variations of the midnight Te at two altitude ranges for F10.7 between 120 and 160 units. Mill Hill empirical model values are represented by the line and circle curves (bottom) for 300 km at 1200 LT with F10.7 = 140 units and (top) for 500 km.

ing the standard deviation over the average. The average F10.7 for the selected data shown at the bottom panels indicates approximately a constant level, so in our discussion here we can ignore the solar activity effect on the ionospheric seasonal change. The well-known semiannual Ne changes are more pronounced in the F2 region, with a slightly larger Ne in spring than in autumn. This equinoctial asymmetry was also seen at the MU radar site in East Asia [*Balan et al.*, 1998], as well as at Millstone Hill (see the line-and-dots in the Ne panel of Figure 3). The semiannual O/N2 and solar zenith angle χ changes may contribute to the asymmetry since O/N2 $\times$ cos χ is larger in spring as indicated in calculations based on the MSIS model [*Hedin*, 1987].

[10] Meanwhile, in the F2 region, Ti also exhibits a weak semiannual variation with equinoctial asymmetries. The semiannual variations in Ti also occur over the MU radar site at high altitudes [*Otsuka et al.*, 1998] and Millstone Hill for low altitudes. The highest Ti occurs in May at St. Santin, as at Millstone (see the line-and-dots in the Ti panel of Figure 3). Such a high Ti implies a high neutral temperature Tn, which can be verified by the MSIS86 model, leading to a higher F2 peak height [*Zhang et al.*, 1999] where the ion loss rate is slower, thus giving rise to a high Ne. Therefore this type of semiannual change (spring-autumn asymmetry) in Tn may contribute also to that in Ne. Increases in the peak height due to a high Tn are much smaller at Millstone Hill due to its higher magnetic dip angle I of $\sim72°$ because the balance height between the chemical loss and diffusion, which the F2 peak height is located around, depends

on $\sin^2 I$ which is associated with the diffusion velocity [*Zhang et al.*, 2003].

[11] As for Te, it is lowest at equinox, opposite to the corresponding Ne maxima. An obvious anticorrelation between Te and Ne [see, e.g., *Bilitza*, 1975; *Mahajan*, 1977; *Schunk and Nagy*, 1978; *Brace and Theis*, 1978; Paper I] can be seen. Unlike at Millstone Hill (see the line-and-dots in the Te panel of Figure 3), the St. Santin Te is higher in winter than in equinox because of the rapid decrease of Ne toward winter. At lower altitudes, since Ne and its semiannual changes are small, the electron cooling changes less and Te closely follows the solar heating variation over a year.

[12] In seasonal variations the local minimum and maximum of the three parameters occur not always to be centered exactly around the equinoctial day. The Ne maximum and the Te minimum in autumn occur ~1 month later from the September equinoctial day, while those in spring occur around the March equinoctial day. This feature is also consistent with the previous work in Japan [*Balan et al.*, 1998; *Kawamura et al.*, 2002].

[13] During the night the seasonal Te variation at St. Santin differs from the one at Millstone (Figure 4). The St. Santin Te is generally higher in summer than in winter. At very high altitudes it becomes almost constant over the year. Millstone observations indicate, however, that at high F2 region heights Te in winter exceeds that in summer (see the line-and-dots curve for Millstone model values at 500 km in the top panel). This high Te phenomenon has been reported before [see, e.g., *Evans*, 1973] and considered to be due to the photoelectron heating from the conjugate ionosphere during the Millstone Hill winter night. The magnetic conjugate latitude for Millstone is $-67°$. This is much higher than that for St. Santin, $-31°$. Then the Millstone Hill conjugate ionosphere experiences longer solar irradiation in Southern Hemisphere summer and is very often still under sunlit when it is around midnight in winter at Millstone, giving a higher Te due to conjugate photoelectron heating. During its winter night, however, the St. Santin ionosphere receives much less photoelectron heating from its conjugate ionosphere, which is largely in darkness, so that the Te enhancement does not occur.

[14] In the yearly variation, as shown in Figure 5 which gives data, yearly averages, and standard deviation error bars at two altitude ranges near noon, Ti and Ne follow the F10.7 change. The F10.7 values are yearly averages over those days when there are ISR data included in the analysis and do not necessarily represent the true yearly F10.7 variation. Ti and Ne are larger in the later solar cycle with a stronger solar maximum. Te variations are more complicated. It tends to decrease toward high solar activity. The yearly variation of Te is not as well patterned as that of the plasma temperature difference, Te-Ti (see discussions in the next section). As seen in Figure 5, the Te-Ti yearly variation tends to be anticorrelated with F10.7 variations, especially over high altitudes, as a result of the Ne effect.

[15] For the altitude variation (Figure 6), Ti increases rapidly up to ~200 km (see circles for data, thin solid lines for averages at various height bins, and error bars for standard deviations on averages), following the neutral temperature Tn change, and then increases fairly slowly between 200 and 400 km giving a reasonable estimate of the
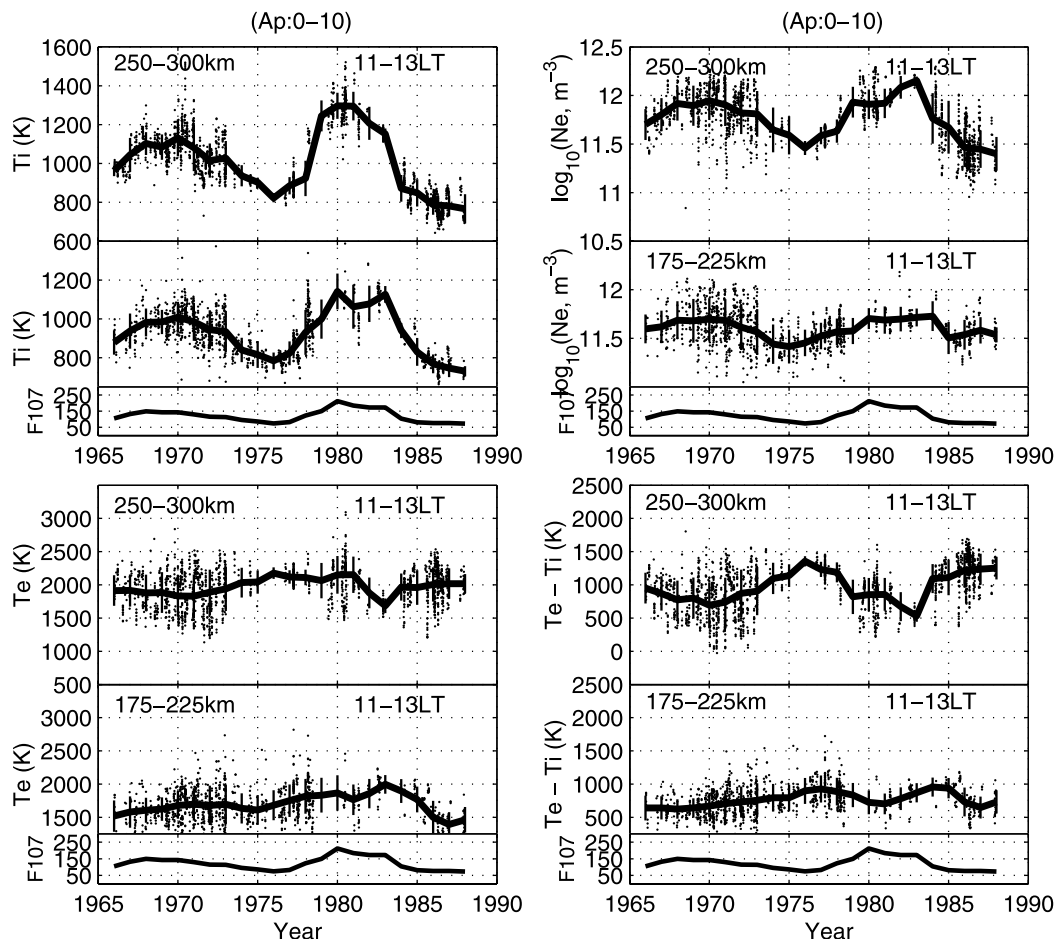
Figure 5. Yearly variations of the midday (top) Ti and Ne and (bottom) Te and Te-Ti at two altitude ranges for F10.7 between 120 and 160 units.

exospheric temperature. It tends to show an increased slope above 400 km which is an indication of the heat flux from the plasmasphere. Te (dots and thick solid lines) has a largely similar height variation pattern for lower solar activity. However, a minimum is formed for high solar activity at ~300 km, in the vicinity of the F2 peak (see Paper I). Obviously, electron cooling effects become significant at high solar activity due to the enhanced Ne. Starting from 1900 LT, the thermal balance between ions and electron is resumed as the nocturnal heating dies out. The balance is established later in time for low solar activity, where the daytime Te and its separation from Ti are relatively large, than for high solar activity. Again, the higher Ne for higher solar activity helps a more efficient establishment of the thermal balance between Te and Ti.

4. Further Discussions on Te

[16] Te variations with solar activity and its dependence on Ne are actually more complicated than the general picture described above. An enhanced solar EUV flux gives rise to more photoelectrons, which in turn elevate plasma temperatures by heating processes (proportional to Ne); meanwhile, the increased electron density due to the enhanced EUV flux leads to an enhanced electron cooling rate through Coulomb collisions (proportional to Ne^2), which

may lead to a lower Te. The actual response of Te to a change in solar EUV is the result of, in addition to effects of heat conduction at high altitudes, these two competing processes, and depends much on the level of background Ne.

[17] The relationship between Te and solar activity (or F10.7) can be quantified using the following expression: $Te = C_0 + C_1 \times f$, where $f = (F10.7 - 135)/100$ is the normalized F10.7, C_0 is the background Te independent of
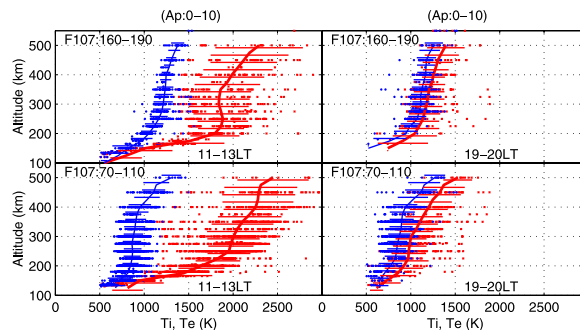

Figure 6. Ti and Te altitude profiles at two local time spans for two solar activity levels. The blue circles are for Ti and the red dots are for Te.
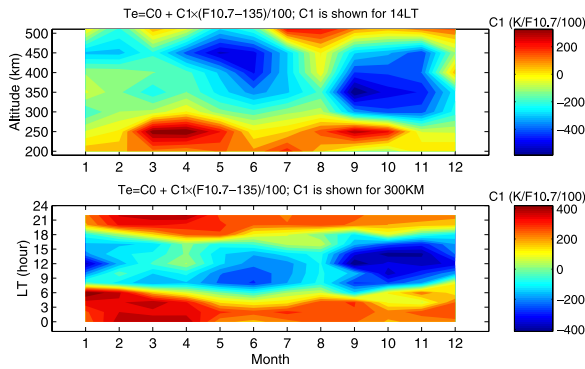
Figure 7. Te dependences on the solar activity at different heights, local times, and months. Coefficient C_1 in $Te = C_0 + C_1 \times f$ is shown, where $f = (F10.7 - 135)/100$ is the normalized F10.7 and C_0 is the background Te independent of solar activity. C_1 represents the slope of the Te change with respect to f change. C_0 and C_1 are obtained by the least-squares fit using the paired Te and f data. C_1 is shown here in the unit of °K per 100 F10.7 units.

Figure 9. Linear relationship between Te-Ti and Nel and the logarithm Ne.

solar activity, and C_1 represents the slope of the Te change with respect to f change. C_0 and C_1 can be obtained by the least-squares fit using the paired Te and f data. It can be seen from Figure 7 that below 300 km, the daytime Te tends to increase toward high solar activity and increases faster in equinox. Above 300 km, it decreases, especially, near equinox. Near the F2 peak altitude (see results for 300 km in Figure 7), Te increases with the solar activity at night while it decreases by day. These results do not quite agree with those from Millstone Hill, especially in summer when Te increases with F10.7 over an entire day [see *Bilitza and Hoegy*, 1990; Paper I]. In fact, as seen in Figure 3, Millstone Hill has a very low Ne between March and September, the cooling effect caused by the enhanced Ne due to the F10.7 increase should be rather weak, and it is the enhanced heating that produces the increase of Te with F10.7.

[18] To further examine the Te-Ne interrelationship, we calculate the linear correlation coefficient using data from all months and years (see Figure 8). The correlation is high when Ne is large (daytime), suggesting the existence of an
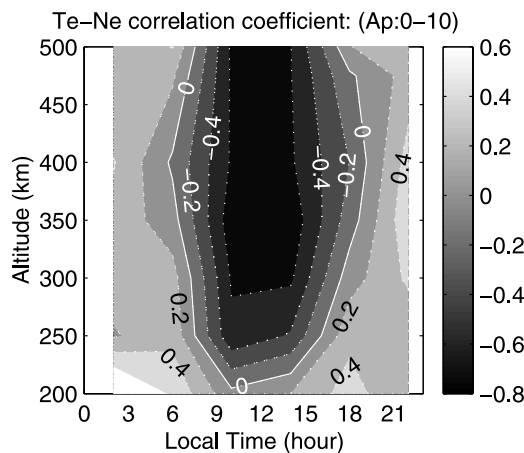
Ne threshold to turn on and off its effects on Te [*Evans*, 1971]. Te does not depend much on Ne at night when Ne is low and the photoelectron heating is largely absent, instead it is controlled mainly by the thermal balance between neutrals, ions, and electrons.

[19] Physically, the plasma temperature difference Te-Ti may be better associated with Ne than is Te in terms of the energy budget, since that difference represents the energy transfer from electrons to ions [*Lejeune*, 1972]. Shown in Figure 9 is the Te-Ti with Nel (logarithm Ne) scatter plot. Nel is preferred here since it has been indicated that it represents better the linear correlation between Te and electron density than Ne itself (see *Bilitza* [1975] and Figure 4a of Paper I). The linear correlation coefficient between Te-Ti and Nel, r(Te-Ti,Nel), for $200-400$ km height range between 1100 and 1300 LT is -0.80, while for Te and Nel, r(Te,Nel) is -0.60. The well-defined Te-Ti with Nel relationship does not change much with season at St. Santin. At Millstone Hill, r(Te-Ti,Nel) $= -0.70$ and r(Te,Nel) $= -0.75$ in December for $250-500$ km height range between $1100-1300$ LT, and in July both are close to -0.1. Apparently, Millstone Hill shows a different temperature-density coupling feature.

5. St. Santin ISR Model

[20] St. Santin ISR empirical models have been created using a bin-fit technique slightly updated from that for Millstone Hill models [*Holt et al.*, 2002]. Measurements of ISR basic parameters Te, Ti, and Ne are binned by month and local time with 3-month and 1-hour bin sizes. Assuming a linear function between any two consecutive altitude nodes (piecewise-linear function), we obtain the height variation with linear coefficients determined subsequently. These nodes are at 100, 110, 120, 130, 140, 160, 180, 200, 225, 250, 300, 350, 400, and 550 km, and these coefficients are assumed to be linear to the solar activity index F10.7, i.e., $P = \beta_0 + \beta_1 \times f$, where P is for either Nel, Te or Ti, the βs are fitting coefficients, and $f = (F10.7 - 135)/100$ is the normalized solar 10.7 cm flux calculated from F10.7 for the previous day. A sequential least squares fit based on

Figure 8. Te-Ne correlation coefficient obtained with data from all months and years.

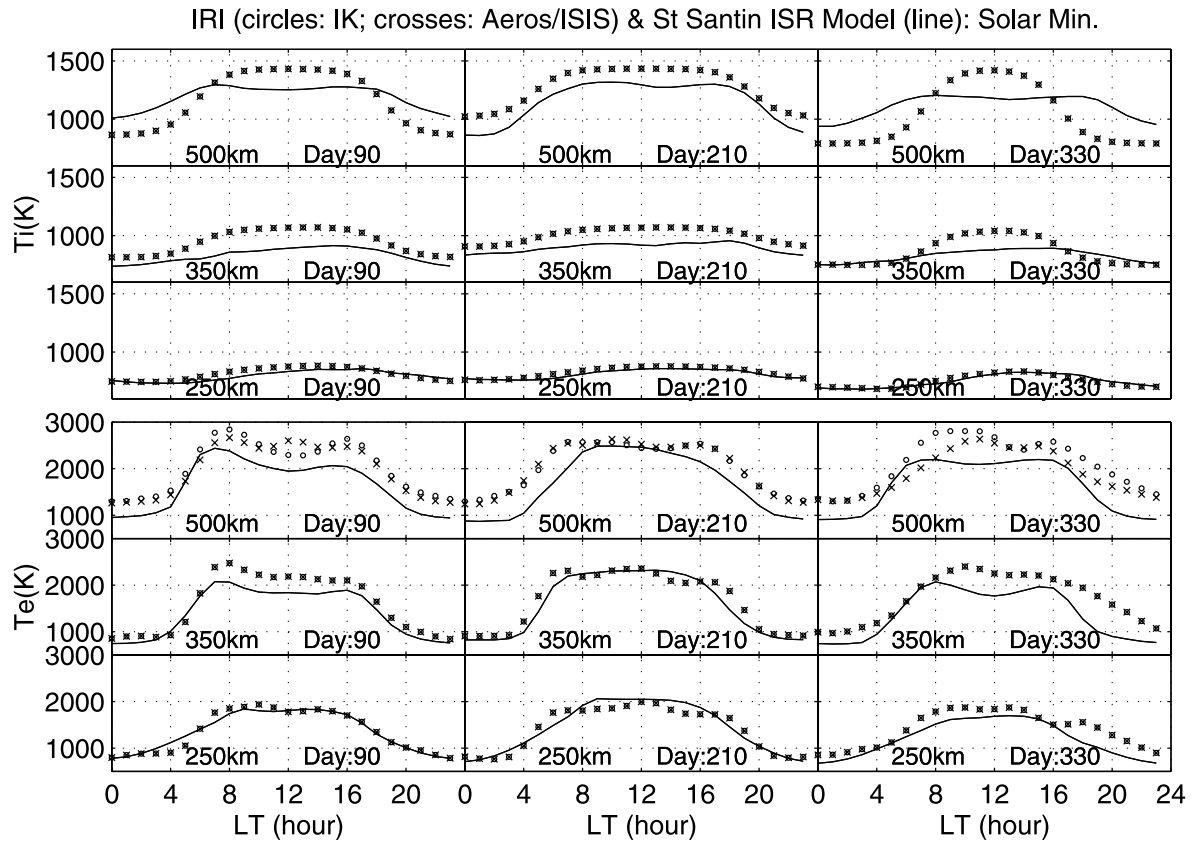**Figure 10.** St. Santin model and IRI model (with different options) comparisons for 1986, a year of low solar activity.

Givens transforms [*Gentleman*, 1973] to the solar activity dependency and piecewise-linear altitude dependency functions is performed for each of the 12 (monthly bins) × 24 (hourly bins) = 288 bins with respect to every ISR parameter. This procedure produces two sets of coefficients (β_0 and β_1) for a given month and local time. Each set contains the piecewise-linear function coefficients for those 14 altitude nodes. To further smooth diurnal and seasonal variations, we apply a 3 (month) × 3 (hour) median filter in local time and season to these β coefficients for all altitude nodes. The geomagnetic activity dependency is not determined here due to the lack of variations in the ap index, in this data, over 80% of which corresponded to ap < 20.

[21] Our models are compared with IRI values for 3 days (days 90, 210, and 330) representing equinox, summer, and winter at low (Figure 10) and high (Figure 11) solar activity. We use the latest IRI2000 model with its two plasma temperature options: the Te and Ti model based on the Aeros/ISIS data [see *Bilitza et al.*, 1985, and references therein] and the Te model based on the Intercosmos satellite data [*Truhlik et al.*, 2000]. Ti for high solar activity agrees well. For low solar activity, agreement is found at low altitudes, yet above 350 km, IRI generally gives larger daytime Ti. The IRI day-night amplitude is larger, in particular, in winter.

[22] Te shows better agreement at lower altitudes. Above 350 km, IRI Te is generally higher than the St. Santin model Te by ∼200°K during the day in winter and spring. IRI

assumes constant Te with solar activity, whereas our Te model indicates a slight increase at 250 km and a slight decrease at 350 km toward increasing solar activity.

[23] The morning enhancement of Te is an important feature of the diurnal variation, as indicated previously in the MU radar data [*Otsuka et al.*, 1998], Millstone Hill data (Paper I), and here for St. Santin. The amplitude of the enhancement varies among these sites where the background Ne and solar zenith angle are different. This feature was not well captured by the previous version of the IRI model [e.g., *Watanabe and Oyama*, 1995; *Oyama et al.*, 1996]. The present study shows, however, that this is now generally reproduced for St Santin by the latest IRI model.

6. Concluding Remarks

[24] The Saint Santin ISR data, collected over two solar cycles from 1966 to 1987, have been analyzed to establish the midlatitude ionospheric climatology, in particular that of the upper atmosphere thermal status, as well as empirical models. In comparison with the Millstone Hill results published previously, variations of Ti and Te with time of the day, season, solar activity, and altitude are discussed. Ti at both sites agrees well. Ti between 250 and 350 km peaks not in summer but around May. The F2 region Te at St. Santin is found to be not as high as at Millstone between later spring and earlier summer, when the St. Santin electron density is relatively higher. The midday Te increases below 300 km with F10.7, as at Millstone Hill. Above 300 km it
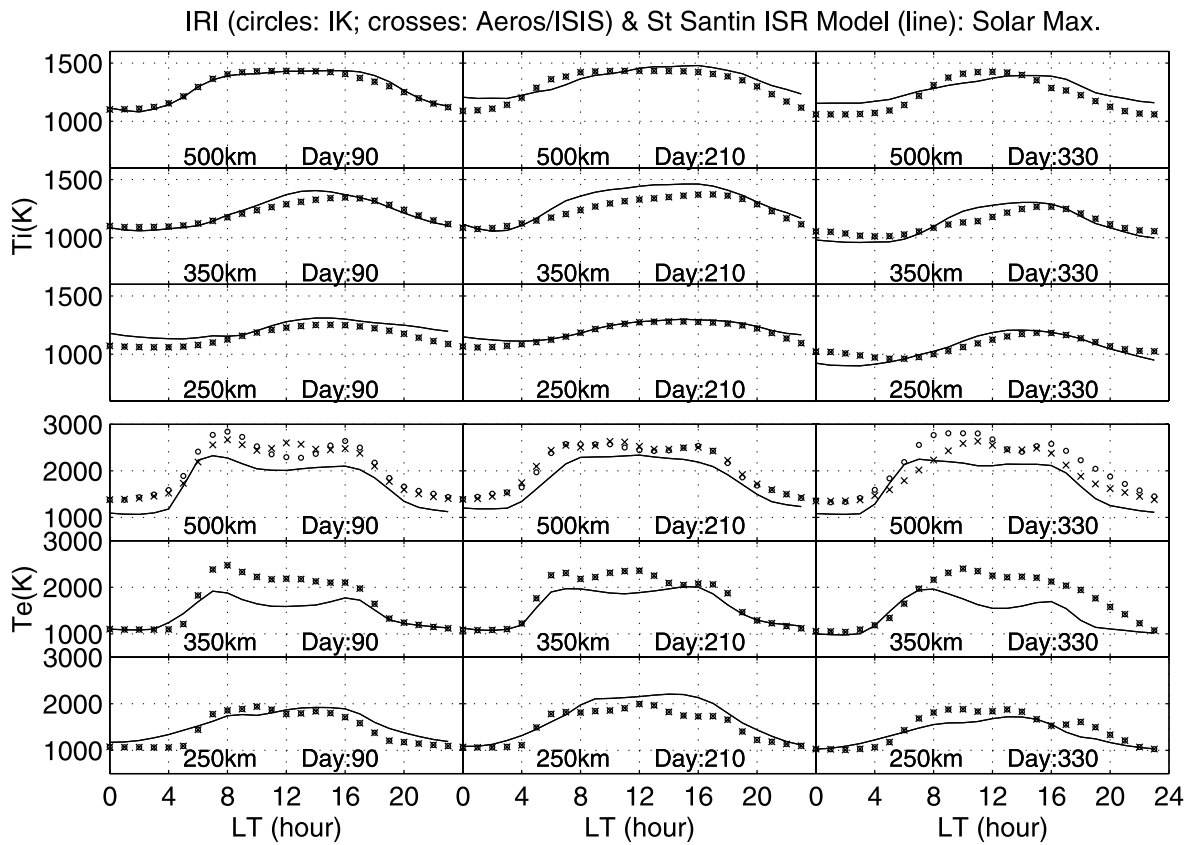
Figure 11. St. Santin model and IRI model (with different options) comparisons for 1989, a year of high solar activity.

tends to decrease with F10.7 at St. Santin, while it increases in summer at Millstone Hill. The anticorrelation between Te-Ti and Nel is higher than that between Te and Nel. Such a Te-Ti and Nel relationship becomes weak for a low Ne so that Te does not depend much on Ne as is the case for summer at Millstone Hill. Comparisons with IRI models indicate good agreement in Ti at high solar activity and in Te and Ti for low altitudes. IRI Te tends to overestimate the St. Santin model values at higher altitudes, e.g., by ~200°K during the day in winter and spring.

References

Alcaydé, D., P. Bauer, A. Hedin, and J. E. Salah (1978), Compatibility of seasonal variations in mid-latitude thermospheric models at solar maximum and low geomagnetic activity, *J. Geophys. Res.*, *83*, 1141–1144.

Balan, N., Y. Otsuka, S. Fukao, and G. J. Bailey (1998), Equinoctial asymmetries in the ionosphere and thermosphere observed by the MU radar, *J. Geophys. Res.*, *103*, 9481–9486.

Bauer, P., P. Waldteufel, and C. Vialle (1974), The French quadristatic incoherent scatter facility, *Radio Sci.*, *9*, 77–83.

Bilitza, D. (1975), Models for the relationship between electron density and temperature in the upper ionosphere, *J. Atmos. Terr. Phys.*, *37*, 1219–1222.

Bilitza, D. (2001), International Reference Ionosphere 2000, *Radio Sci.*, *36*, 261–275.

Bilitza, D., and W. R. Hoegy (1990), Solar activity variations of ionospheric plasma temperatures, *Adv. Space Res.*, *10*(8), 81–90.

Bilitza, D., L. Brace, and R. Theis (1985), Modelling of ionospheric temperature profiles, *Adv. Space Res.*, *5*(7), 53–58.

Brace, L. H., and R. F. Theis (1978), An empirical model of the interrelationship of electron temperature and density in the daytime thermosphere at solar minimum, *Geophys. Res. Lett.*, *5*, 275–278.

Buonsanto, M. J., and L. M. Pohlman (1998), Climatology of neutral exospheric temperature above Millstone Hill, *J. Geophys. Res.*, *103*, 23,381–23,392.

Evans, J. V. (1971), Millstone Hill Thomson scatter results for 1967, *Tech. Rep. 482*, Lincoln Lab., Mass. Inst. of Tech., Lexington, Mass.

Evans, J. V. (1973), Seasonal and sunspot cycle variation of F region electron temperatures and protonospheric heat flux, *J. Geophys. Res.*, *78*, 2344–2349.

Gentleman, W. V. (1973), Least squares computations by Givens transformations without square roots, *J. Inst. Math. Applics.*, *12*, 325–336.

Hedin, A. E. (1987), MSIS-86 thermospheric model, *J. Geophys. Res.*, *92*, 4649–4662.

Holt, J. M., S.-R. Zhang, and M. J. Buonsanto (2002), Regional and local ionospheric models based on Millstone Hill incoherent scatter radar data, *Geophys. Res. Lett.*, *29*(9), 1358, doi:10.1029/2001GL013579.

Kawamura, S., N. Balan, Y. Otsuka, and S. Fukao (2002), Annual and semiannual variations of the midlatitude ionosphere under low solar activity, *J. Geophys. Res.*, *107*(A8), 1166, doi:10.1029/2001JA000267.

Lejeune, G. (1972), The coupling between electron density and electron temperature in the daytime F-region, *Ann. Geophys.*, *28*, 15–20.

Lejeune, G., and M. Petit (1969), A study of the daytime electron temperature, *Planet. Space Sci.*, *17*, 1763–1780.

Lejeune, G., and P. Waldteufel (1970), Mise en évidence de lois empiriques reliant localement la température et la densité électroniques dens la région F de l'ionosphère, *Ann. Geophys.*, *26*, 223–227.

Mahajan, K. K. (1977), Models of electron temperature in the ionospheric F-region using electron density height profiles, *J. Atmos. Terr. Phys.*, *39*, 637–639.

Mazaudier, C., and P. Bauer (1976), Nocturnal thermal disequilibrium of the F2 region ionosphere at middle latitudes, *J. Geophys. Res.*, *81*, 3447–3451.

McPherson, P. H., and W. L. Oliver (1997), F-region temperatures at Malvern and St. Santin, *J. Atmos. Terr. Phys.*, *39*, 779–786.

Otsuka, Y., S. Kawamura, N. Balan, S. Fukao, and G. J. Bailey (1998), Plasma temperature variations in the ionosphere over the middle and upper atmosphere radar, *J. Geophys. Res.*, *103*, 20,705–20,713.

Oyama, K.-I., S. Watanabe, Y. Su, T. Takahashi, and K. Hirao (1996), Seasonal, local time, and longitude variations of electron temperature at the height of ~600 km in the low latitude region, *Adv. Space Res.*, *18*, 269–278.

Rishbeth, H. (1998), How the thermospheric circulation affects the ionospheric F2-layer, *J. Atmos. Sol. Terr. Phys.*, *60*, 1385–1402.

Roemer, M. (1967), Geomagnetic activity effect and 27-day variation: Responses time of the thermosphere and lower exosphere, *Space Res.*, *VII*, 1091–1099.

Salah, J. E., J. V. Evans, D. Alcaydé, and P. Bauer (1976), Comparison of exospheric temperatures at Millstone Hill and St-Santin, *Ann. Geophys.*, *32*, 257–266.

Schunk, R. W., and A. F. Nagy (1978), Electron temperatures in the F region ionosphere: Theory and observations, *Rev. Geophys.*, *16*, 355–399.

Truhlik, V. L., Triskova, J. Smilauer, and V. Afonin (2000), Global empirical model of electron temperatures in the outer ionosphere for period of high solar activity based on data of Intercosmos satellites, *Adv. Space Res.*, *25*(1), 163–172.

Watanabe, S., and K.-I. Oyama (1995), Dynamic model and observation of the equatorial ionosphere, *Adv. Space Res.*, *15*, 109–112.

Zhang, S.-R., and J. M. Holt (2004), Ionospheric plasma temperatures during 1976–2001 over Millstone Hill, *Adv. Space Res.*, *33*, 963–969, doi:10.1016/j.asr.2003.07.012.

Zhang, S.-R., S. Fukao, W. L. Oliver, and Y. Otsuka (1999), The height of the maximum ionospheric electron density over the MU radar, *J. Atmos. Sol. Terr. Phys.*, *61*, 1367–1383.

Zhang, S.-R., W. L. Oliver, J. M. Holt, and S. Fukao (2003), Ionospheric data assimilation: Comparison of extracted parameters using full density profiles and key parameters, *J. Geophys. Res.*, *108*(A3), 1131, doi:10.1029/2002JA009521.

————————

C. Amory-Mazaudier, Centre for the Study of Earth and Planets Environments (CETP), CNRS, 94107 Saint-Maur-des-Fossés Cedex, France. (christine.mazaudier@cetp.ipsl.fr)

J. M. Holt and S.-R. Zhang, Haystack Observatory, Massachusetts Institute of Technology, Route 40, Westford, MA 01886, USA. (jmh@haystack.mit.edu; shunrong@haystack.mit.edu)

A. M. Zalucha, Department of Earth, Atmospheric, and Planetary Sciences, Massachusetts Institute of Technology, Cambridge, MA 02139, USA. (azalucha@mit.edu)